Stem Cell Research & Therapy

RESEARCH Open Access

# N-CADHERIN$^{+}$/CD168$^{-}$ subpopulation determines therapeutic variations of UC-MSCs for cardiac repair after myocardial infarction

Yukang Wu[1†], Jianguo Li[1†], Ke Feng[1], Ailing Tan[1], Yingying Gao[1], Wen Chen[1], Wenwen Jia[1], Xudong Guo[1*] and Jiuhong Kang[1*]

## Abstract

**Background** The efficiency of mesenchymal stem cells (MSCs) in treating myocardial infarction (MI) remains inconsistent, which limits their therapeutic applications. Therefore, exploring the mechanism for the inconsistent efficacy of MSCs and identification the criteria for screening MSCs are important for improving the efficiency of MSCs.

**Methods** Mouse model after MI was utilized to test the role of MSCs from different donors and the functional subpopulation in improving cardiac function. Heterogeneity of MSCs was identified using single-cell RNA sequencing (scRNA-seq) of MSC-GY. GSEA and Scissor analyses were used to find the functional subpopulations of MSCs that promote angiogenesis. The role of functional subpopulations in promoting angiogenesis was verified by detecting the secretory proteins, the ratio of N-CADHERIN$^{+}$/CD168$^{-}$ subpopulations in MSCs, and the tube formation, migration, and proliferation of HUVECs after treatment with conditional medium (CM) derived from different MSCs.

**Results** We found that umbilical cord-derived MSCs (UC-MSCs) from different donors have varied therapeutic efficacy in MI mice and UC-MSCs with higher therapeutic effectiveness exhibited the most potent pro-angiogenic effects by secreting elevated levels of angiogenesis-related proteins, such as MYDGF, VEGFA, and FGF2. ScRNA-seq of 10,463 UC-MSCs revealed that the N-CADHERIN$^{+}$/CD168$^{-}$ subpopulation was closely associated with pro-angiogenic effects, and the ratio of this cell subpopulation was positively correlated with the angiogenic potential of MSCs. We also found that the N-CADHERIN$^{+}$/CD168$^{-}$ subpopulation was the functional subpopulation of MSCs in improving cardiac function of MI mice.

**Conclusions** Our study identified that the N-CADHERIN$^{+}$/CD168$^{-}$ subpopulation was the functional subpopulation of MSCs in treating MI, which was essential for the development and utilization of MSCs in MI treatment.

**Keywords** MSCs, Myocardial infarction, ScRNA-seq, N-CADHERIN$^{+}$/CD168$^{-}$, Angiogenesis

†Yukang Wu and Jianguo Li have contributed equally to this work.

*Correspondence:
Xudong Guo
19504@tongji.edu.cn
Jiuhong Kang
jhkang@tongji.edu.cn

## Introduction

Myocardial infarction (MI) involves extensive death of cardiomyocytes due to coronary artery occlusion, leading to impaired cardiac function and progressive heart failure [1]. The transplantation of mesenchymal stem cells (MSCs) has emerged as a promising therapeutic strategy for treating MI, attributed to their low immunogenicity and paracrine effects, as demonstrated in animal studies and clinical trials [2, 3]. Lee and Amado demonstrated that MSC transplantation significantly reduced myocardial injury and improved cardiac function in the infarcted hearts of mice and pigs, respectively [4, 5]. A meta-analysis by Lalu et al. of 23 clinical trials (involving 1,148 patients) confirmed that MSC application was safe and effective for treating MI [6]. Additionally, Chullikana et al. found that MSC transplantation improved ejection fraction and reduced adverse cardiac events in MI patients [7]. However, Nowbar et al. reported the limited effects of MSCs on improving left ventricular ejection fraction (LVEF) based on an analysis of clinical trial data from 1252 patients [8]. Thus, achieving consistent and effective MSC treatment for MI remains a critical challenge.

Single-cell RNA sequencing (scRNA-seq) enables characterization of gene expression at the single-cell level and resolves cellular heterogeneity of MSCs. MSCs have been reported to be a heterogeneous population, with different cellular subpopulations have varying biological properties [9–12]. Sacchetti and Zhou et al. found that $CD146^+$ and $LepR^+$ MSCs, highly expressed bone-related genes, exhibited significant osteogenic differentiation ability [13, 14]. Similarly, Arufe and Mifune et al. identified the $CD271^+$ MSCs possessed high expression of cartilage-related genes and significant chondrogenic differentiation ability [15, 16]. Additionally, the $CMKLR1^+$ MSCs have been reported to possess strong immunomodulatory and osteogenic capabilities [17]. Thus, understanding the heterogeneity of MSCs would be crucial for identifying MSC subpopulations suitable for treating specific diseases. However, it remains unclear whether specific MSC subpopulation could improve the treatment efficacy for MI.

The paracrine effects have been identified as a major mechanism of MSCs for the treatment of MI [2, 18, 19]. MSCs can secrete anti-inflammatory factors such as tumor necrosis factor stimulated gene 6 (TSG6), transforming growth factor beta 1 (TGF-β1), and interleukin 10 (IL10), which regulate macrophage polarization and inhibit T cell activation [20]. Lee et al. also found that MSCs improved cardiac function by regulating the inflammatory response, which was blocked by TSG6 knockdown [4]. Furthermore, the angiogenesis-related factors such as vascular endothelial growth factor (VEGF), fibroblast growth factor 2 (FGF2), and hepatocyte growth factor (HGF) were secreted by MSCs to promote angiogenesis and cell survival [21, 22]. Lee et al. has also demonstrated that the pro-angiogenic effect is the main mechanism by which MSCs improve cardiac function and enhance therapeutic efficacy for treating MI [23]. Despite these insights, the key mechanism influencing MSC efficacy for MI treatment remains unclear.

In this study, we demonstrated that variations in the angiogenic potential of MSCs affected their therapeutic efficacy in MI mice. Furthermore, we identified the $N\text{-}CADHERIN^+/CD168^-$ subpopulation as a functional MSC subpopulation in regulating angiogenesis and improving the heart function of MI mice, with the ratio of this subpopulation significantly correlating with the therapeutic effects of MSCs. Thus, our study highlights a specific MSC subpopulation that improving the heart function of MI mice, which is essential for the development and utilization of MSCs in MI treatment.

## Methods

### Experimental animals

The C57BL/6 male mice (6–8 weeks old) used in this study were purchased from Shanghai Laboratory Animal Center (SLAC), Shanghai, China. Mice were housed in the Laboratory Animal Research Center, Tongji University, and maintained under controlled temperature (22 °C ± 1 °C) and humidity conditions with a 12:12 h light:darkness cycle. Mice were euthanized by cervical dislocation and the death was confirmed by cardiorespiratory arrest. All animal experiments were conducted following the institutional animal ethics guidelines and were approved by the Animal Use Committee of Tongji University (TJAB04523102).

### Cell culture

UC-MSCs were cultured in MSC medium (ScienCell #7501) supplemented with 5% FBS, 1 × mesenchymal stem cell growth supplement (MSCGS), and 1 × penicillin/streptomycin (PS) solution.

### Construction of MI model and UC-MSC transplantation

Animals were randomly assigned to different cage locations to prevent positional effects. To establish a mouse model of MI, adult male C57BL/6 mice were anesthetized with 2% isoflurane inhalation, followed by ligation of the left main descending coronary artery (LCA), as previously described [24]. Immediately after MI, $2 \times 10^5$ UC-MSCs suspended in 30 μL saline were injected intramyocardially into the infarct border zone at three distinct sites. Control MI animals received saline injection only, while sham-operated animals underwent all

surgical procedures except for LCA ligation and intramyocardial injection.

In the experiment evaluating the therapeutic effects of MSCs from different donors on MI, 38 adult male C57BL/6 mice were randomly assigned to the following groups: the Sham group (n = 7), the MI + Saline group (n = 7, with 2 mice dying during surgery, 7/9), the MI + MSC-CX group (n = 7, injected with $2 \times 10^5$ MSC-CX, with 1 mouse dying during surgery, 7/8), the MI + MSC-CJ group (n = 7, injected with $2 \times 10^5$ MSC-CJ), and the MI + MSC-GY group (n = 7, injected with $2 \times 10^5$ MSC-GY). A total of 35 mice survived, resulting in a survival rate of 92.1%. After evaluation on day 3, all 28 surviving infarcted mice had an LVEF below 40%.

In the experiment evaluating the therapeutic impact of N-CADHERIN$^+$/CD168$^-$ subpopulation within MSCs on MI, 30 adult male C57BL/6 mice were randomly assigned to the following groups: the MI + Saline group (n = 6, with 2 mice dying during surgery, 6/8), the MI + N-CADHERIN$^+$/CD168$^-$ MSC-GY group (n = 6, injected with sorted N-CADHERIN$^+$/CD168$^-$ cells from MSC-GY, with 2 mice dying during surgery, 6/8), the MI + others group (n = 6, injected with remaining MSC-GY cells excluding the N-CADHERIN$^+$/CD168$^-$ subpopulation, with 1 mice dying during surgery, 6/7), and the MI + N-CADHERIN$^+$/CD168$^-$ MSC-CX group (n = 6, injected with sorted N-CADHERIN$^+$/CD168$^-$ cells from MSC-CX, with 1 mice dying during surgery, 6/7). A total of 24 mice survived, resulting in a survival rate of 80%. After evaluation on day 3, all 24 surviving infarcted mice had a LVEF below 40%.

In both experiments, all surgeries and injections were performed by a single experienced operator in a blinded manner. Additionally, The LVEF measurements and data analyses were conducted with the investigator blinded to the group assignments, ensuring unbiased assessment of cardiac function across all groups.

#### Assessment of cardiac function

Echocardiography was performed to assess the cardiac function of MI mice 28 days after cell transplantation (Visual Sonics Vevo 2100 system equipped with a 40-MHz 550 s probe). LVEF, fraction shortening, end-diastolic diameter, end-systolic diameter were measured and calculated using cardiac echocardiography software [25].

#### Masson trichrome staining

Masson trichrome staining was performed as previously described [24, 26]. Briefly, the mouse hearts (4 weeks after MI) were fixed in 4% paraformaldehyde for 24 h at 4 °C and then dehydrated using a sucrose gradient. Hearts were sectioned from below the ligation site to the apex at 8 μm thickness, with samples taken at 500 μm intervals for staining (Yeasen). Infarct size was quantified as the average of five sections using the formula: infarct size = [infarct perimeter (infarct epicardium + infarct endocardium) × 100]/left ventricle perimeter (left ventricle epicardium + left ventricle endocardium).

#### Immunostaining

Immunostaining was performed as previously described [27]. Fixed slides were blocked for 1 h at room temperature in PBS containing 10% donkey serum and 0.1% Triton X-100. Slides were incubated overnight at 4 °C with primary antibodies, followed by incubation with fluorescent secondary antibodies and Hoechst33342 for nuclear staining at room temperature for 1 h. CD31 and α-SMA positive cells were quantified from three randomly selected sections per slide.

#### Flow cytometry (FACS)

UC-MSCs were dissociated with TrypLE (Gibco), washed with PBS, and $3 \times 10^5$ cells were incubated with 100 μL PBS containing 1 μL CD168 (RHAMM)-FITC antibody (bs-4736R-FITC, Bioss) and 10 μL CDH2 (N-CADHERIN)-PE antibody (11039-R001-PE, Sino Biological) for 30 min at 4 °C. Cells were analyzed using a BD FACSVerse, and data were processed with FlowJo software. For sorting of the N-CADHERIN$^+$/CD168$^-$ MSC subpopulation. MSCs were stained with CD168 (RHAMM)-FITC antibody (4 μL/$10^6$ cells) and CDH2 (N-CADHERIN)-PE antibody (30 μL/$10^6$ cells) for 30 min at 4 °C. After washing with PBS, the N-CADHERIN$^+$/CD168$^-$ subpopulation was sorted by BD FACSAria II.

#### Tracing of MSCs

MSCs were transfected with lipophilic tracker-DiR (DiIC18(7)) (APEx BIO, B8806; 10 μM in PBS) labeling for 20 min before implantation into the hearts. At day 1 and 7 after transplantation, mice were anesthetized with isoflurane and photographed with an IVIS Lumina XRMS Series III instrument. The region of interest (ROI) of DiR-labeled MSCs was measured using living image4.4 software (Radiant Efficiency).

#### Production of UC-MSCs conditioned medium

UC-MSCs ($2 \times 10^6$ cells) from different donors were cultured in 10 cm dishes until 80–90% confluent. Cells were washed with PBS and switched to low glucose DMEM. After 5 days, supernatants were collected and stored at 4 °C for further use.

### Tube formation assay

Tube formation assay was performed as previously described [22]. Basement membrane matrix (Matrigel®, BD Biosciences) was solidified in 24-well plates at 37 °C for 30 min. HUVECs ($8\times10^4$ cells/well) were plated on Matrigel in 1640 medium with 10% FBS and 30% conditioned medium from UC-MSCs. Tube formation was imaged after 8 h, and structures were quantified using Image J.

### Cell migration assay

HUVECs ($4\times10^4$ cells/well) were cultured in 24-well plates for 24 h. After creating a scratch, cells were cultured in RPMI 1640 medium with 30% UC-MSC conditioned medium for 16 h. Images of migrated cells were taken at 0, 8, and 16 h, and the migration rate was calculated using Image J.

### Cell proliferation assay

HUVECs ($8\times10^4$ cells/well) were cultured in 12-well plates in RPMI 1640 medium with 30% UC-MSC conditioned medium for 48 h. Cell numbers were counted at 0, 24, and 48 h using CounterStar software.

### scRNA-seq analysis

Single-cell RNA sequencing was conducted using 10 × Genomics technology. Data were processed into a Seurat object, filtering out cells with fewer than 200 features or more than 5% mitochondrial gene expression. Data normalization and feature selection identified 2,000 highly variable features. Principal Component Analysis (PCA) reduced dimensionality to 30 components, which were used for clustering at a resolution of 0.25. UMAP and t-SNE techniques visualized cell populations.

### Statistical analysis

All data were presented as mean ± S.E.M. of three independent experiments. Statistical significance was determined using one-way ANOVA with Tukey's post hoc test for more than two groups (GraphPad Prism software). The significance levels were set at $^{*}$, $^{\#}P<0.05$, $^{**}$, $^{\#\#}P<0.01$, and $^{***}$, $^{\#\#\#}P<0.001$. The work had been reported in line with the ARRIVE guidelines 2.0.

## Results

### MSCs from different donors exhibit distinct effects on improving cardiac function in mice post-MI

We obtained UC-MSCs from three donors (MSC-GY, MSC-CJ, and MSC-CX), with flow cytometry results showed that these UC-MSCs were positive for CD44, CD90, CD105, and CD73, while negative for CD34 and HLA-DR (Fig. 1A). We then transplanted these three UC-MSCs into MI mice hearts via intramyocardial injection. Four weeks post-transplantation, echocardiography was performed to evaluate the cardiac function. Our results demonstrated that MSC-GY and MSC-CJ significantly improved LVEF and left ventricular fraction shortening (LVFS). Correspondingly, we observed a decrease in left ventricular internal diameter in diastole (LVIDd) and systole (LVIDs) in the mice transplanted with MSC-GY and MSC-CJ, whereas MSC-CX transplantation had no effect on cardiac function post-MI (Figs. 1B, 1C and S1). Additionally, the Masson's trichrome staining revealed that MSC-GY and MSC-CJ transplantation reduced the injury area in the MI mice (Fig. 1D). Quantification of DiR-labeled MSCs revealed that MSC-GY and MSC-CJ exhibited a higher retention ratio compared to MSC-CX (Fig. S2). These results indicated that UC-MSCs derived from different donor exhibit variations in therapeutic efficacy in mice post-MI.

### Variable angiogenic efficacies of MSCs from different donors

MSCs could promote angiogenesis and reduce inflammation. Vagnozzi et al. found that intramyocardial injection of both live and cryopreserved MSCs resulted in the accumulation of $CCR2^+$ and $CX3CR1^+$ macrophage, which alleviated inflammation in mice post-MI [28]. Based on this, we hypothesized that angiogenesis might be the primary mechanism affecting MSC efficacy in treating MI. We examined MSC-induced angiogenesis via CD31 and α-smooth muscle actin (α-SMA) immunostaining and observed that MSC-GY and MSC-CJ significantly increased α-SMA and CD31-positive cells in peri-infarct heart regions, while MSC-CX had minimal impact (Fig. 2A and B). To further validate the angiogenic effects of different MSCs, we treated human umbilical vein endothelial cells (HUVECs) with conditional medium (CM) derived from different MSCs. Results showed that the MSC-GY and MSC-CJ CM significantly enhanced the tube formation, migration, and proliferation of HUVECs, rather than the MSC-CX CM (Fig. 2C–E), consistent with the results in the MI model. We then performed the secretome analysis of three UC-MSCs CM. Gene Ontology (GO) and Gene Set Enrichment Analysis (GSEA) results indicated that upregulated secretory factors in MSC-GY and MSC-CJ CM were associated with endothelial cell proliferation, vascular development, and endothelial cell migration (Fig. 2F, Fig. S3 and S4). Angiogenic factors such as VEGF and FGF2 were significantly higher in the CM of MSC-GY and MSC-CJ compared to MSC-CX (Fig. 2G). These results

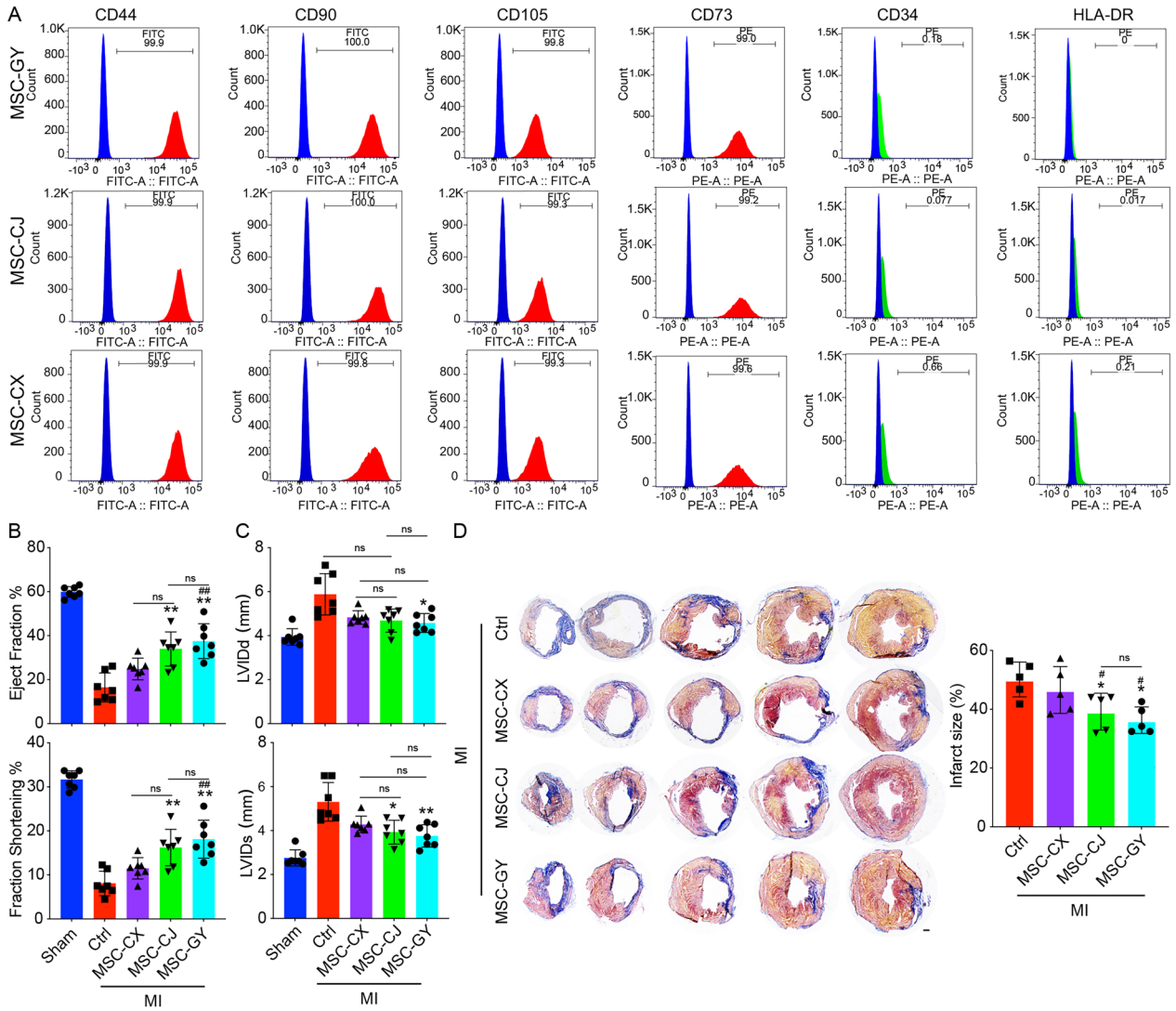


**Fig. 1** MSCs from Different Donors Exhibit Distinct Effects on Improving Cardiac Function in Mice Post-MI. (**A**) Flow cytometric analysis of UC-MSCs from different donors, showing MSC-positive markers (CD44, CD90, CD105, and CD73) and MSC-negative markers (CD34 and HLA-DR). (**B**) Echocardiography analysis of ejection fraction (EF) and fraction shortening (FS) in Sham, MI, MI + MSC-CX, MI + MSC-CJ, and MI + MSC-GY at 4 weeks post-MI (n = 7). $^{**}P < 0.01$ versus Ctrl; $^{\#\#}P < 0.01$ versus MSC-CX. (**C**) Echocardiographic analysis of left ventricular end-diastolic diameter (LVIDd) and left ventricular end-systolic diameter (LVIDs) in Sham, MI, MI + MSC-CX, MI + MSC-CJ, and MI + MSC-GY at 4 weeks post-MI (n = 7). $^{*}P < 0.05$, $^{**}P < 0.01$ versus Ctrl. (**D**) Representative images of Masson trichrome staining of hearts sections (left) and quantification of infarct size (right) at 4 weeks post-MI. $^{*}P < 0.01$ versus Ctrl; $^{\#}P < 0.05$ versus MSC-CX. Statistical significance was determined using one-way ANOVA followed by Tukey's post hoc. Scale bar: 500 μm

(See figure on next page.)

**Fig. 2** Variable Angiogenic Efficacies of MSCs from Different Donors. (**A** and **B**) Representative immunostaining images for CD31 and α-SMA in the border zone of infarcted hearts at 4 weeks post-MI (**A**) and statistical analysis (**B**). $^{***}P < 0.001$ versus Ctrl; $^{\#} < 0.05$, $^{\#\#}P < 0.01$ versus MSC-CX. (**C**) Representative images illustrating the tube formation of HUVECs on Matrigel and statistical analysis. $^{***}P < 0.001$ versus Ctrl; $^{\#\#\#}P < 0.001$ versus MSC-CX. (**D**) Representative images depicting HUVEC migration and statistical analysis. $^{**}P < 0.01$, $^{***}P < 0.001$ versus Ctrl; $^{\#\#}P < 0.0,1$ $^{\#\#\#}P < 0.001$ versus MSC-CX; ns versus MSC-CJ. (**E**) Statistical analysis of HUVEC proliferation treated with conditional medium (CM) from UC-MSCs. $^{**}P < 0.01$ versus Ctrl; ns versus MSC-CJ. (**F**) GO term analysis highlighting the secreted proteins highly expressed in the CM of MSC-GY and MSC-CJ. (**G**) Heatmap illustrating the expression levels of angiogenesis-related factors in the CM of MSC-GY, MSC-CJ, and MSC-CX. Statistical significance assessed using one-way ANOVA followed by Tukey's post hoc. Scale bar: 100 μm

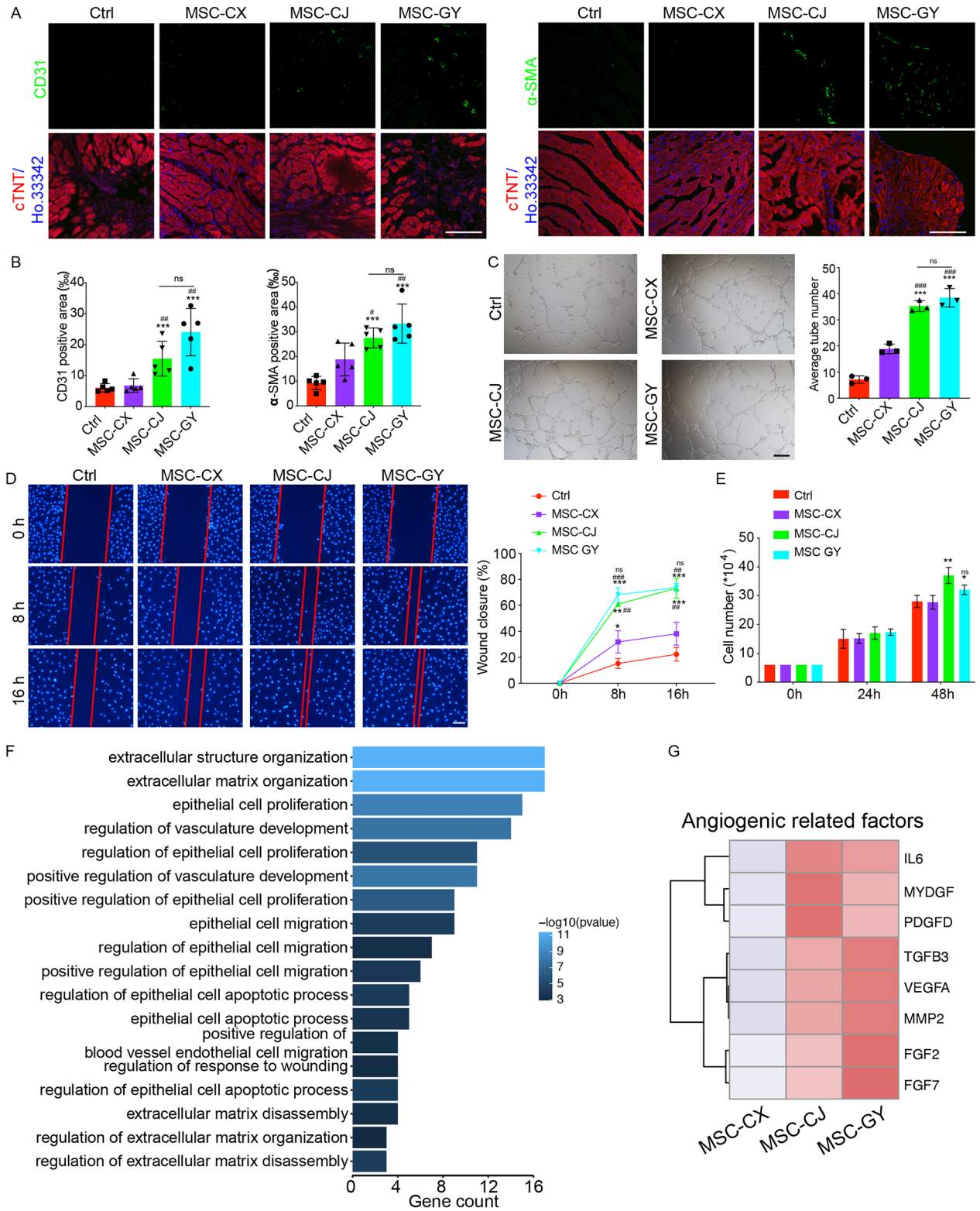


**Fig. 2** (See legend on previous page.)

suggested that the angiogenic capacity of MSCs influences their efficacy in MI treatment.

### Single-cell transcriptomic analysis reveals four major subpopulations within MSCs

To explore the heterogeneity of UC-MSCs, we generated single-cell transcriptome profiles of MSC-GY, which exhibited the most significant therapeutic effects in MI treatment. After quality control, single-cell transcriptomes of 10,463 cells were acquired for further analysis. By analyzing variably expressed genes across all cells, we identified four clusters of MSCs: Cluster 1 (35.10%), Cluster 2 (27.85%), Cluster 3 (23.06%), and Cluster 4 (13.99%) (Fig. 3A). We then performed differential gene expression analysis to find unique signatures for each cluster, presenting the top 10 significantly differentially expressed (SDE) genes of each cluster (Fig. 3B).

To reveal the biological functions of each cluster, we performed the GSEA of cluster-specific differentially expressed genes (DEGs). The results showed that Cluster 1 was significantly associated with vascular development, smooth muscle cell migration and adhesion, indicating that Cluster 1 might regulate angiogenesis. Cluster 2 showed enrichment in metabolic processes such as lipid metabolism and fatty acid metabolism, while Cluster 3 was associated with cell morphogenesis and cell junction assembly, and Cluster 4 was linked to cell proliferation-related biological processes such as cell division and microtubule polymerization or depolymerization. Based on their gene expression profiles and pathway enrichment analysis, we named Cluster 1 as the angiogenesis subpopulation, Cluster 2 as the metabolic regulation subpopulation, Cluster 3 as the niche support subpopulation, and Cluster 4 as the proliferation subpopulation (Fig. 3C).

Furthermore, we predicted the cell cycle phases of each cell and found that cells in the proliferation subpopulation were predominantly in the G2/M phase, confirming the strong proliferative capacity of this subpopulation (Fig. 3D). The proposed trajectory analysis can infer the evolution of cell subpopulation by their expression characteristics. We performed pseudo-time reconstruction of MSC-GY to stratify the connection of each sub-population. Pseudo-time reconstruction revealed seven cell states, starting from state 7 and ending at state 1. The angiogenesis subpopulation served as the starting point of the trajectory, while the metabolic regulation, niche support, and proliferation subpopulation were mainly located at the terminal end (Fig. 3E). This pattern showed that the angiogenesis subpopulation also represents the stem-like cell subpopulation within UC-MSCs, which gradually transits into other subpopulations.

### The N-CADHERIN$^+$/CD168$^-$ subpopulation is associated with the angiogenesis capacity of MSCs

To identify the cell subpopulations associated with angiogenesis, we integrated single-cell RNA-seq data of MSC-GY with RNA-seq data from MSC-M01 and M02 in GSE13491 by Scissor analysis [29], which can identify the most phenotypically relevant cells from single-cell data. MSC-M02 in Lee et al. significantly promoted the angiogenesis in the heart of rats after MI. In this integrated analysis [23], Scissor identified 1890 Scissor$^+$ cells with gene expression profiles similar to MSC-M02 (Fig. 4A), suggesting that these 1890 Scissor$^+$ cells in the single-cell data were similar to MSC-M02, which could promote angiogenesis and improve heart function post- MI. Statistical analysis showed that 1824 (96.5%) of these Scissor$^+$ cells originated from the angiogenesis subpopulation (Fig. 4B). Therefore, we concluded that the angiogenesis subpopulation is the functional component of MSCs that can promote angiogenesis and improve heart function in the MI model.

Next, we performed a comprehensive analysis between the cell surface proteins and DEGs in the angiogenesis subpopulation, finding that the angiogenesis subpopulation was positive for N-CADHERIN and negative for CD168 (Fig. 4C). Analysis of data from GSE165811 [30] revealed that CD168 was negatively correlated with the expression levels of angiogenesis-related genes such as VEGFA and FGF2, while N-CADHERIN was positively correlated with these genes (Fig. 4D). Additionally, analysis of single-cell data (GSE182158) [31] showed that genes highly expressed in the N-CADHERIN$^+$/CD168$^-$ cell subpopulation were associated with angiogenesis (Fig. 4E–H). These results indicated that N-CADHERIN$^+$/CD168$^-$ subpopulation is significantly associated with promoting angiogenesis of MSCs.

(See figure on next page.)

**Fig. 3** Single-cell Transcriptomic Analysis Reveals Four Major Subpopulations within MSCs. (**A**) tSNE plot illustrating the clustering of 10,463 cells from MSC-GY (above), along with the statistical analysis indicating the distribution of cells in each subpopulation (below). (**B**) Heatmap displaying the top 10 marker genes for each subpopulation. (**C**) GSEA-KEGG showing the enriched pathway for each subpopulation. (**D**) tSNE plot demonstrating the distribution of each subpopulation across the cell cycle. (**E**) Pseudotime analysis reflecting the cell state transition and differentiation trajectories of these four subpopulations

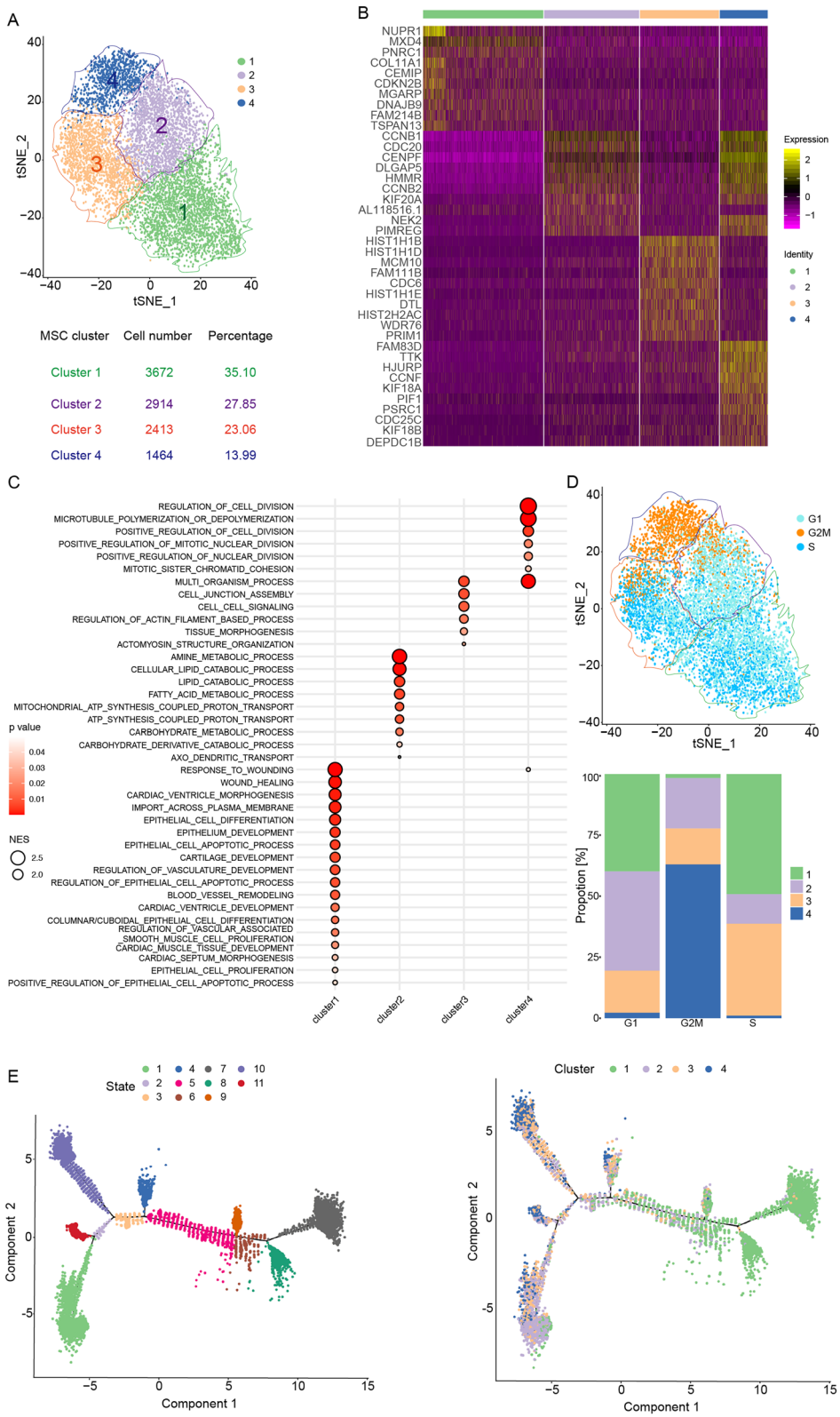


**Fig. 3** (See legend on previous page.)

### N-CADHERIN$^+$/CD168$^-$ cell subpopulation have beneficial effects on cardiac function of MI mice

To elucidate the relationship between the proportion of N-CADHERIN$^+$/CD168$^-$ cell subpopulation and the function of UC-MSCs in MI, we detected the ratio of N-CADHERIN$^+$/CD168$^-$ subpopulation in three UC-MSCs. Flow cytometry analysis revealed that the ratio of the N-CADHERIN$^+$/CD168$^-$ cell subpopulation in MSC-CX was significantly lower than that in MSC-GY and MSC-CJ (Fig. 5A and B). Correlation analysis also showed a positive correlation between the proportion of N-CADHERIN$^+$/CD168$^-$ cells and the improvement of cardiac function across MSC-GY, MSC-CJ, and MSC-CX (Fig. 5C). These results indicated that the ratio of the N-CADHERIN$^+$/CD168$^-$ subpopulation affects the efficiency of MSCs in treating MI. To explore the role of N-CADHERIN$^+$/CD168$^-$ cell subpopulation on the cardiac function in mice after MI, we sorted out the N-CADHERIN$^+$/CD168$^-$ MSC subpopulation from MSC-GY (Fig. S5), and our results showed that the N-CADHERIN$^+$/CD168$^-$ subpopulation significantly improved heart function and reduced fibrosis in MI mice. In contrast, the other MSCs depleted of N-CADHERIN$^+$/CD168$^-$ subpopulation failed in improving heart function of MI mice (Figs. 5D–F and S6), suggesting that the N-CADHERIN$^+$/CD168$^-$ MSC subpopulation were indeed the functional subpopulation responsible for the therapeutic effect in treating MI. In addition, we also found that the N-CADHERIN$^+$/CD168$^-$ cells from MSC-CX could improve heart function and reduce fibrosis (Figs. 5D–F and S6), which further supporting the consistent therapeutic role of N-CADHERIN$^+$/CD168$^-$ cells in treating MI.

To identify the key upstream regulators maintaining the N-CADHERIN$^+$/CD168$^-$ subpopulation, we reconstructed gene regulatory networks using SCENIC [32] and explored the unique transcriptional regulation of DEGs in distinct subpopulations. We found that the angiogenesis subpopulation might be regulated by the transcription factors CEBPB, TCF21, and TAL1 (Fig. 5G and H). These results suggested that CEBPB, TCF21, and TAL1 may maintain the fate of the N-CADHERIN$^+$/CD168$^-$ subpopulation and increase the ratio of N-CADHERIN$^+$/CD168$^-$ subpopulation in MSCs.

## Discussion

MSCs hold significant promise for MI therapy, yet growing evidence reveals inconsistent therapeutic efficacy among MSCs derived from different donors [8, 33–35]. Our study identified critical differences in the therapeutic potential of UC-MSCs from various donors, highlighting that the pro-angiogenic capacity of MSCs was a determinant of their efficacy in MI treatment. Given the variability in donor-derived MSCs used in clinical settings, our findings suggested that selecting MSCs with higher pro-angiogenic potential is essential for achieving more effective clinical outcomes.

Paracrine effects are the primary mechanism by which MSCs confer therapeutic benefits in MI. Lee et al. demonstrated that MSCs enhanced cardiac function in MI mice through the secretion of TSG6, which modulated inflammatory responses [4]. Additional studies emphasized the secretion of angiogenesis-related factors as a crucial mechanism. Hu et al. showed that pre-conditioning MSCs under hypoxic conditions (0.5% oxygen for 24 h) significantly elevated the levels of VEGF and other angiogenic factors, thereby enhancing angiogenesis in the infarct border zone, reducing cardiac fibrosis, and improving cardiac function in MI mice [36]. Overexpressing the factors like VEGF and FGF2 had been shown to significantly boost the angiogenic potential of MSCs, thus improving their reparative capacity in damaged hearts after MI [37, 38]. Our findings corroborated that effective MSCs secrete higher levels of pro-angiogenic factors, supporting the notion that enhancing angiogenesis via paracrine effects of MSCs is the key to improve cardiac function post-MI.

ScRNA-seq enables detailed characterization of cellular expression profiles, offering an invaluable tool for exploring MSC heterogeneity [39]. Recent studies have identified MSC transcriptome profiles based on the DEGs and differential pathways, without functional analysis of subpopulations. Some studies failed to define the functional subpopulations because of insufficient cell numbers. Huang et al. analyzed only 361 UC-MSCs and found that the heterogeneity was primarily influenced by cell cycle differences [40], Hou et al. [41] and Wolock et al. [42] respectively identified the subpopulations in UC-MSCs and bone marrow MSCs, highlighting the differences

(See figure on next page.)

**Fig. 4** The N-CADHERIN$^+$/CD168$^-$ Subpopulation is Associated with the Angiogenesis Capacity of MSCs (**A**) tSNE plot illustrating the Scissor-selected cells associated with the therapeutic effect of MSCs in MI treatment, accompanied by statistical analysis. (**B**) Expression levels of N-CADHERIN and CD168 in Scissor$^+$ cells compared to other cells. (**C**) tSNE plot showing the expression pattern of N-CADHERIN and CD168 in MSC-GY. (**D**) Pearson correlation analysis of N-CADHERHN and CD168 expression levels with angiogenesis-related gene expression. (**E**) tSNE plot illustrating the clustering of 9,039 cells from GSE182158. (**F**) tSNE plot displaying the expression pattern of N-CADHERIN and CD168 in GSE182158. (**G** and **H**) GO term analysis of up-regulated genes (**G**) and down-regulated genes (**H**) in the N-CADHERIN$^+$/CD168$^-$ subpopulation

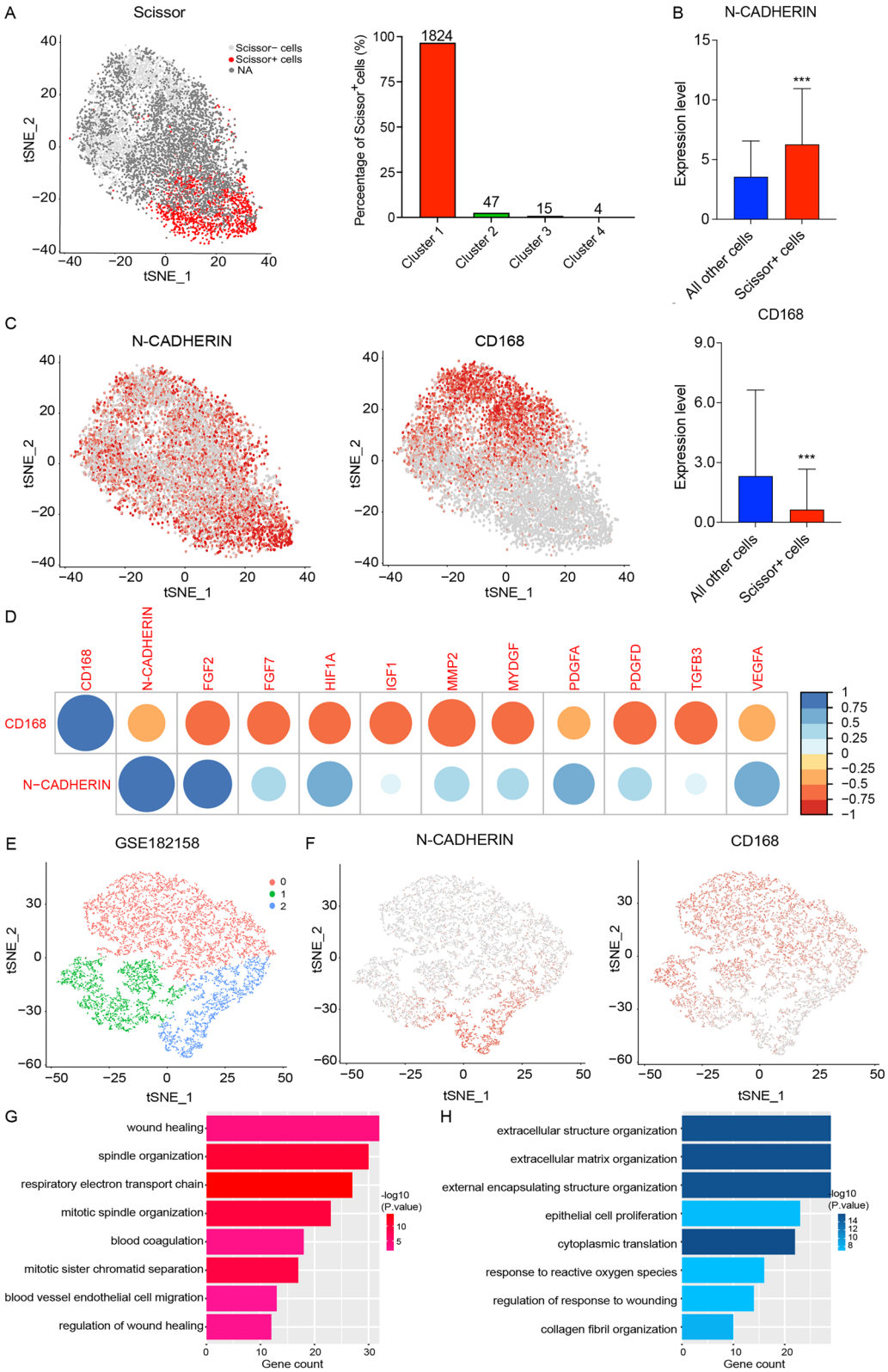


**Fig. 4** (See legend on previous page.)

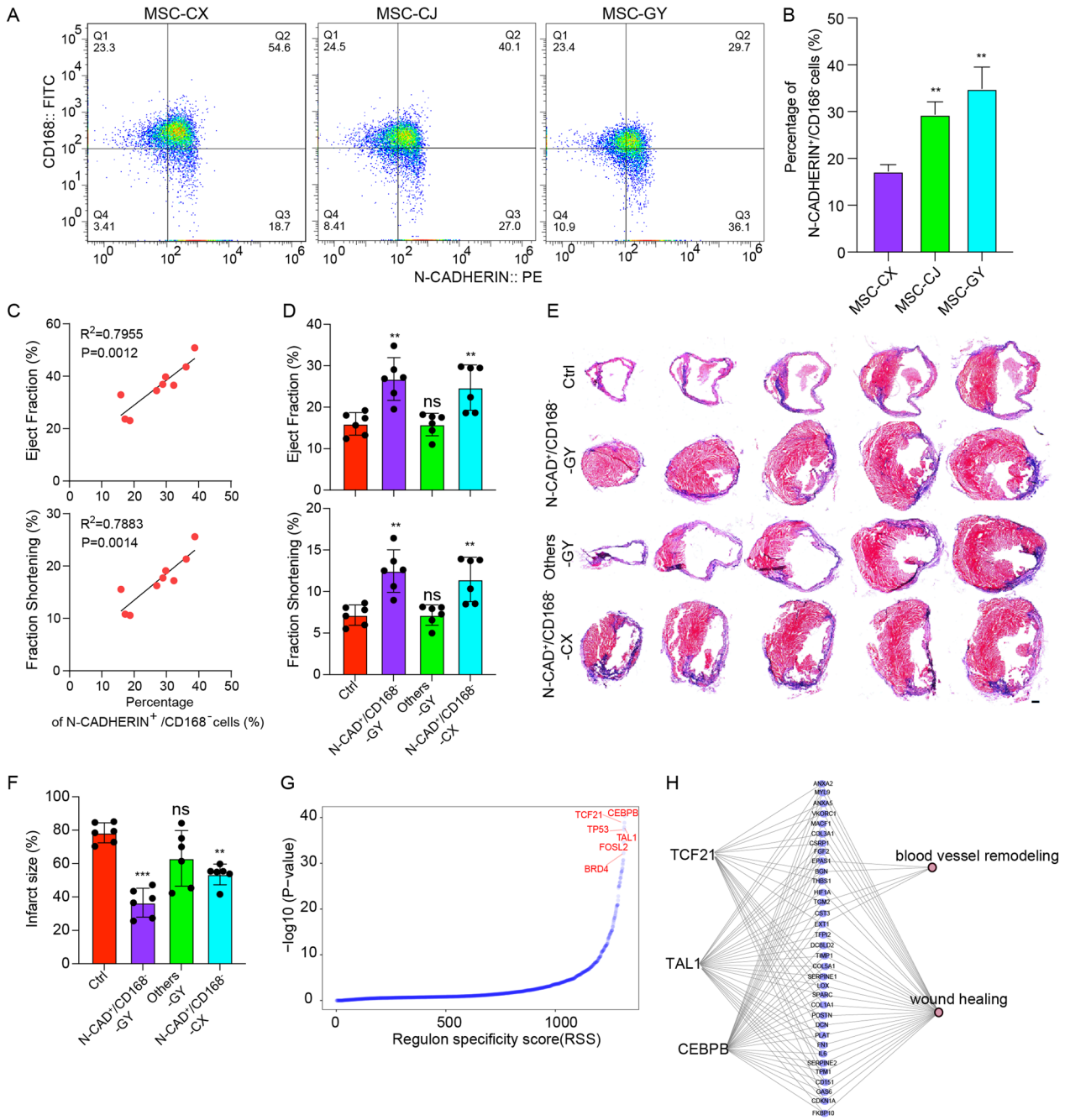


**Fig. 5** N-CADHERIN$^+$/CD168$^-$ Cell Subpopulation Have Beneficial Effects on Cardiac Function of MI Mice. (**A** and **B**) Representative images depicting the percentage of N-CADHERIN$^+$/CD168$^-$ subpopulation in the UC-MSCs from different donors (**A**), with quantitative analysis of percentages of cells (**B**). $^{**}P < 0.01$, $^{***}P < 0.001$ versus MSC-CX. (**C**) Pearson correlation analysis of EF and FS with the percentage of N-CADHERIN$^+$/CD168$^-$ cells. (**D**) Echocardiography analysis of EF and FS in MI (Ctrl), MI + N-CADHERIN$^+$/CD168$^-$ from MSC-GY (N-CAD$^+$/CD168$^-$-GY), MI + MSC-GY depleted of N-CADHERIN$^+$/CD168$^-$ subpopulation (Others-GY), and MI + N-CADHERIN$^+$/CD168$^-$ from MSC-CX (N-CAD$^+$/CD168$^-$-CX) groups at 4 weeks post-MI (n = 6). ns, $^{**}P < 0.01$, versus Ctrl. (**E**) Representative images of masson trichrome staining of heart sections at 4 weeks post-MI. Scale bar: 500 μm. (**F**) Quantification of infarct size at 4 weeks post-MI. ns, $^{**}P < 0.01$, versus Ctrl. (**G**) Ranked results of the DEGs in the N-CADHERIN $^+$/CD168$^-$ subpopulation. (**H**) Prediction of transcription factors (TFs) for the N-CADHERIN$^+$/CD168$^-$ subpopulation. Statistical significance was determined using one-way ANOVA followed by Tukey's post hoc

in differentiation potentials. In this study, we expanded the analysis to 10,463 UC-MSCs, identifying four main subpopulations. Notably, the N-CADHERIN$^+$/CD168$^-$ subpopulation emerged as a key functional group in regulating angiogenesis. We found that N-CADHERIN$^+$/CD168$^-$ subpopulation was the functional MSCs in improving heart function of MI mice, and the ratio of this subpopulation was positively correlated with the pro-angiogenic effects of MSCs. Together, our study demonstrated that variations in angiogenic potential influence the therapeutic efficacy of UC-MSCs in MI treatment.

This study has several limitations. First, our study found that the N-CADHERIN$^+$/CD168$^-$ subpopulation was significantly associated with the pro-angiogenic capacity of MSCs and their efficacy in MI mice, which needed to be confirmed in a large animal model of MI (eg, swine or nonhuman primates) and quantified to determine the relationship between the ratio of the N-CADHERIN$^+$/CD168$^-$ cell subpopulation and the efficacy of MSCs, providing a basis for improving the clinical application of MSCs. Second, we found that CEBPB, TCF21, and TAL1 may maintain the fate of N-CADHERIN$^+$/CD168$^-$ subpopulation, but have not yet examined whether CEBPB, TCF21, and TAL1 can increase the ratio of functional cell subpopulations in MSCs. We will evaluate the role of these factors in future studies.

## Conclusion

In summary, by exploring UC-MSC heterogeneity, we identified the N-CADHERIN$^+$/CD168$^-$ subpopulation as crucial for the regulation of angiogenesis and cardiac function recovery in MI mice. The ratio of this subpopulation determined the angiogenic efficacy of UC-MSCs, providing a basis for selecting MSCs suitable for MI therapy. This finding deepened the understanding of UC-MSC heterogeneity and established a new criteria for screening MSCs for effective MI treatment.

### Abbreviations

| | |
|---|---|
| MSCs | Mesenchymal stem cells |
| MI | Myocardial infarction |
| scRNA-seq | Single-cell RNA sequencing |
| TSG6 | Tumor necrosis factor stimulated gene 6 |
| TGF-β1 | Transforming growth factor beta 1 |
| IL10 | Interleukin 10 |
| VEGF | Vascular endothelial growth factor |
| FGF2 | Fibroblast growth factor 2 |
| HGF | Hepatocyte growth factor |
| LVEF | Left ventricular ejection fraction |
| LVFS | Left ventricular fraction shortening |
| LVIDd | Left ventricular internal diameter in diastole |
| LVIDs | Left ventricular internal diameter in systole |
| α-SMA | α-Smooth muscle actin |
| HUVECs | Human umbilical vein endothelial cells |
| CM | Conditional medium |
| GO | Gene ontology |
| GSEA | Gene set enrichment analysis |
| SDE | Significantly differentially expressed |
| DEGs | Differentially expressed genes |
| SLAC | Shanghai laboratory animal center |
| MSCGS | Mesenchymal stem cell growth supplement |
| PS | Penicillin/streptomycin |
| LCA | Left main descending coronary artery |
| EF | Ejection fraction |
| FS | Fraction shortening |
| PCA | Principal component analysis |

## Supplementary Information

The online version contains supplementary material available at https://doi.org/10.1186/s13287-024-04032-4.

Additional file 1.

### Acknowledgements

We thank Shanghai East Hospital for providing UC-MSCs. The authors declare that they have not used Artificial Intelligence in this study.

### Author contributions

YW, J L, KF, AT, YG, WC, WJ, XG and JK designed the overall study, including biological experiments and bioinformatics analysis. YW, J L, XG and JK wrote the manuscript YW and KF performed the biological experiments. JL and YW performed data analyses. AT carried out the random allocation process. All authors discussed the study results and worked together on preparing and editing the manuscript.

### Funding

This study was supported by grants from the National Key R&D Program of China (2021YFA1100400), the National Natural Science Foundation of China (82271723, 82071728, and 32170575), the Natural Science Foundation of Shanghai (23ZR1465500), and the Fundamental Research Funds for the Central Universities (22120220620).

### Availability of data and materials

All data generated or analyzed during this study are included in this manuscript and its Supplementary Information files. The scRNA-seq and proteomics data have been deposited in the Genome Sequence Archive for Human database (HRA007901). The source data presented in this study are available from the corresponding author upon request.

## Declarations

### Ethical approval and consent to participate

This study was approved by the Animal Experimentation Ethics Committee, Tongji University [TJABO4523102 (title: The functions and mechanisms of N-CADHERIN$^+$/CD168$^-$ umbilical cord mesenchymal stem cell subpopulation in the treatment of myocardial infarction; date:28 $^{th}$ Feb, 2023)] and approved by the Institutional Animal Care and Use Committee of Tongji University. Human umbilical cord mesenchymal stem cells were obtained following signed informed consent and approved for the project: The preparation and construction of clinical human umbilical cord and umbilical cord blood stem cells, the Ethics Committee of Shanghai East Hospital (No: 2017 Preliminary Review No. (001)). 18th Oct. 2019.

### Consent for publication

Not applicable.

### Competing interests

Authors declare that they have no competing interests.

### Author details

[1]Clinical and Translational Research Center of Shanghai First Maternity and Infant Hospital, Shanghai Key Laboratory of Maternal Fetal Medicine, Shanghai Key Laboratory of Signaling and Disease Research, Frontier Science Center for Stem Cell Research, National Stem Cell Translational Resource Center, School of Life Sciences and Technology, Tongji University, Shanghai, China.

Received: 27 June 2024 Accepted: 30 October 2024
Published online: 13 November 2024

**References**


1. Dreyer RP, Zheng X, Xu X, et al. Sex differences in health outcomes at one year following acute myocardial infarction: a report from the China Patient-Centered Evaluative Assessment of Cardiac Events prospective acute myocardial infarction study. Eur Heart J-Acute Ca. 2019;8(3):273–82.
2. Bagno L, Hatzistergos KE, Balkan W, et al. Mesenchymal stem cell-based therapy for cardiovascular disease: progress and challenges. Mol Ther. 2018;26(7):1610–23.
3. Williams AR, Hare JM. Mesenchymal stem cells: biology, pathophysiology, translational findings, and therapeutic implications for cardiac disease. Circ Res. 2011;109(8):923–40.
4. Lee RH, Pulin AA, Seo MJ, et al. Intravenous hMSCs improve myocardial infarction in mice because cells embolized in lung are activated to secrete the anti-inflammatory protein TSG-6. Cell Stem Cell. 2009;5(1):54–63.
5. Amado LC, Saliaris AP, Schuleri KH, et al. Cardiac repair with intramyocardial injection of allogeneic mesenchymal stem cells after myocardial infarction. Proc Natl Acad Sci U S A. 2005;102(32):11474–9.
6. Lalu MM, Mazzarello S, Zlepnig J, et al. Safety and efficacy of adult stem cell therapy for acute myocardial infarction and ischemic heart failure (SafeCell Heart): a systematic review and meta-analysis. Stem Cell Transl Med. 2018;7(12):857–66.
7. Chullikana A, Sen Majumdar A, Gottipamula S, et al. Randomized, double-blind, phase I/II study of intravenous allogeneic mesenchymal stromal cells in acute myocardial infarction. Cytotherapy. 2015;17(3):250–61.
8. Nowbar AN, Mielewczik M, Karavassilis M et al. Discrepancies in autologous bone marrow stem cell trials and enhancement of ejection fraction (DAMA-SCENE): weighted regression and meta-analysis. Bmj-Brit Med J 2014;348.
9. Zhang C, Han X, Liu J, et al. Single-cell transcriptomic analysis reveals the cellular heterogeneity of mesenchymal stem cells. Genom Proteom Bioinform. 2022;20(1):70–86.
10. Zhang P, Dong J, Fan X, et al. Characterization of mesenchymal stem cells in human fetal bone marrow by single-cell transcriptomic and functional analysis. Signal Transduct Target Ther. 2023;8(1):126.
11. Zhang YY, Li F, Zeng XK, et al. Single cell RNA sequencing reveals mesenchymal heterogeneity and critical functions of Cd271 in tooth development. World J Stem Cells. 2023;15(6):589–606.
12. Miura T, Kouno T, Takano M, et al. Single-cell RNA-Seq Reveals LRRC75A-expressing cell population involved in VEGF secretion of multipotent mesenchymal stromal/stem cells under ischemia. Stem Cells Transl Med. 2023;12(6):379–90.
13. Sacchetti B, Funari A, Michienzi S, et al. Self-renewing osteoprogenitors in bone marrow sinusoids can organize a hematopoietic microenvironment. Cell. 2007;131(2):324–36.
14. Zhou BO, Yue R, Murphy MM, et al. Leptin-receptor-expressing mesenchymal stromal cells represent the main source of bone formed by adult bone marrow. Cell Stem Cell. 2014;15(2):154–68.
15. Arufe MC, De la Fuente A, Fuentes I, et al. Chondrogenic potential of subpopulations of cells expressing mesenchymal stem cell markers derived from human synovial membranes. J Cell Biochem. 2010;111(4):834–45.
16. Mifune Y, Matsumoto T, Murasawa S, et al. Therapeutic superiority for cartilage repair by CD271-positive marrow stromal cell transplantation. Cell Transplant. 2013;22(7):1201–11.
17. Xie Z, Yu W, Ye G, et al. Single-cell RNA sequencing analysis of human bone-marrow-derived mesenchymal stem cells and functional subpopulation identification. Exp Mol Med. 2022;54(4):483–92.
18. Shi W, Xin Q, Yuan R, et al. Neovascularization: the main mechanism of MSCs in ischemic heart disease therapy. Front Cardiovasc Med. 2021;8: 633300.
19. Sun SJ, Wei R, Li F, et al. Mesenchymal stromal cell-derived exosomes in cardiac regeneration and repair. Stem Cell Rep. 2021;16(7):1662–73.
20. Shi Y, Wang Y, Li Q, et al. Immunoregulatory mechanisms of mesenchymal stem and stromal cells in inflammatory diseases. Nat Rev Nephrol. 2018;14(8):493–507.
21. Kwon HM, Hur SM, Park KY, et al. Multiple paracrine factors secreted by mesenchymal stem cells contribute to angiogenesis. Vascul Pharmacol. 2014;63(1):19–28.
22. Park SJ, Kim RY, Park BW, et al. Dual stem cell therapy synergistically improves cardiac function and vascular regeneration following myocardial infarction. Nat Commun. 2019;10(1):3123.
23. Lee EJ, Choi EK, Kang SK, et al. N-cadherin determines individual variations in the therapeutic efficacy of human umbilical cord blood-derived mesenchymal stem cells in a rat model of myocardial infarction. Mol Ther. 2012;20(1):155–67.
24. Wu Y, Guo X, Han T, et al. Cmarr/miR-540-3p axis promotes cardiomyocyte maturation transition by orchestrating Dtna expression. Mol Ther Nucleic Acids. 2022;29:481–97.
25. Guo X, Xu Y, Wang Z, et al. A Linc1405/eomes complex promotes cardiac mesoderm specification and cardiogenesis. Cell Stem Cell. 2018;22(6):893-908e896.
26. Feng K, Wu Y, Li J, et al. Critical role of miR-130b-5p in cardiomyocyte proliferation and cardiac repair in mice after myocardial infarction. Stem Cells. 2024;42(1):29–41.
27. Xi J, Wu Y, Li G, et al. Mir-29b mediates the neural tube versus neural crest fate decision during embryonic stem cell neural differentiation. Stem Cell Rep. 2017;9(2):571–86.
28. Vagnozzi RJ, Maillet M, Sargent MA, et al. An acute immune response underlies the benefit of cardiac stem cell therapy. Nature. 2020;577(7790):405–9.
29. Sun D, Guan X, Moran AE, et al. Identifying phenotype-associated subpopulations by integrating bulk and single-cell sequencing data. Nat Biotechnol. 2022;40(4):527–38.
30. Zhang C, Zhou L, Wang Z, et al. Eradication of specific donor-dependent variations of mesenchymal stem cells in immunomodulation to enhance therapeutic values. Cell Death Dis. 2021;12(4):357.
31. Wang Z, Chai C, Wang R, et al. Single-cell transcriptome atlas of human mesenchymal stem cells exploring cellular heterogeneity. Clin Transl Med. 2021;11(12): e650.
32. Aibar S, Gonzalez-Blas CB, Moerman T, et al. SCENIC: single-cell regulatory network inference and clustering. Nat Methods. 2017;14(11):1083–6.
33. Cho HM, Lee KH, Shen YM, et al. Transplantation of hMSCs genome edited with LEF1 improves cardio-protective effects in myocardial infarction. Mol Ther Nucleic Acids. 2020;19:1186–97.
34. Yan W, Lin C, Guo Y, et al. N-cadherin overexpression mobilizes the protective effects of mesenchymal stromal cells against ischemic heart injury through a beta-catenin-dependent manner. Circ Res. 2020;126(7):857–74.
35. Lei J, Wang S, Kang W, et al. FOXO3-engineered human mesenchymal progenitor cells efficiently promote cardiac repair after myocardial infarction. Protein Cell. 2021;12(2):145–51.
36. Hu X, Xu Y, Zhong Z, et al. A large-scale investigation of hypoxia-preconditioned allogeneic mesenchymal stem cells for myocardial repair in nonhuman primates: paracrine activity without remuscularization. Circ Res. 2016;118(6):970–83.
37. Karpov AA, Udalova DV, Pliss MG, et al. Can the outcomes of mesenchymal stem cell-based therapy for myocardial infarction be improved? Providing weapons and armour to cells. Cell Proliferat. 2017. https://doi.org/10.1111/cpr.12316.
38. Bagno LL, Carvalho D, Mesquita F, et al. Sustained IGF-1 secretion by adipose-derived stem cells improves infarcted heart function. Cell Transpl. 2016;25(9):1609–22.
39. Chen P, Tang S, Li M, et al. Single-cell and spatial transcriptomics decodes Wharton's Jelly-derived mesenchymal stem cells heterogeneity and a subpopulation with wound repair signatures. Adv Sci (Weinh). 2023;10(4): e2204786.
40. Huang Y, Li Q, Zhang K, et al. Single cell transcriptomic analysis of human mesenchymal stem cells reveals limited heterogeneity. Cell Death Dis. 2019;10(5):368.
41. Hou WH, Duan L, Huang CY, et al. Cross-tissue characterization of heterogeneities of mesenchymal stem cells and their differentiation potentials. Front Cell Dev Biol. 2021. https://doi.org/10.3389/fcell.2021.781021.
42. Wolock SL, Krishnan I, Tenen DE, et al. Mapping distinct bone marrow niche populations and their differentiation paths. Cell Reps. 2019;28(2):302.


## Publisher's Note

# Terms and Conditions

Springer Nature journal content, brought to you courtesy of Springer Nature Customer Service Center GmbH (“Springer Nature”).
Springer Nature supports a reasonable amount of sharing of research papers by authors, subscribers and authorised users (“Users”), for small-scale personal, non-commercial use provided that all copyright, trade and service marks and other proprietary notices are maintained. By accessing, sharing, receiving or otherwise using the Springer Nature journal content you agree to these terms of use (“Terms”). For these purposes, Springer Nature considers academic use (by researchers and students) to be non-commercial.
These Terms are supplementary and will apply in addition to any applicable website terms and conditions, a relevant site licence or a personal subscription. These Terms will prevail over any conflict or ambiguity with regards to the relevant terms, a site licence or a personal subscription (to the extent of the conflict or ambiguity only). For Creative Commons-licensed articles, the terms of the Creative Commons license used will apply.
We collect and use personal data to provide access to the Springer Nature journal content. We may also use these personal data internally within ResearchGate and Springer Nature and as agreed share it, in an anonymised way, for purposes of tracking, analysis and reporting. We will not otherwise disclose your personal data outside the ResearchGate or the Springer Nature group of companies unless we have your permission as detailed in the Privacy Policy.
While Users may use the Springer Nature journal content for small scale, personal non-commercial use, it is important to note that Users may not:

1. use such content for the purpose of providing other users with access on a regular or large scale basis or as a means to circumvent access control;
2. use such content where to do so would be considered a criminal or statutory offence in any jurisdiction, or gives rise to civil liability, or is otherwise unlawful;
3. falsely or misleadingly imply or suggest endorsement, approval , sponsorship, or association unless explicitly agreed to by Springer Nature in writing;
4. use bots or other automated methods to access the content or redirect messages
5. override any security feature or exclusionary protocol; or
6. share the content in order to create substitute for Springer Nature products or services or a systematic database of Springer Nature journal content.

In line with the restriction against commercial use, Springer Nature does not permit the creation of a product or service that creates revenue, royalties, rent or income from our content or its inclusion as part of a paid for service or for other commercial gain. Springer Nature journal content cannot be used for inter-library loans and librarians may not upload Springer Nature journal content on a large scale into their, or any other, institutional repository.
These terms of use are reviewed regularly and may be amended at any time. Springer Nature is not obligated to publish any information or content on this website and may remove it or features or functionality at our sole discretion, at any time with or without notice. Springer Nature may revoke this licence to you at any time and remove access to any copies of the Springer Nature journal content which have been saved.
To the fullest extent permitted by law, Springer Nature makes no warranties, representations or guarantees to Users, either express or implied with respect to the Springer nature journal content and all parties disclaim and waive any implied warranties or warranties imposed by law, including merchantability or fitness for any particular purpose.
Please note that these rights do not automatically extend to content, data or other material published by Springer Nature that may be licensed from third parties.
If you would like to use or distribute our Springer Nature journal content to a wider audience or on a regular basis or in any other manner not expressly permitted by these Terms, please contact Springer Nature at

onlineservice@springernature.com